Natural Resources Research, Vol. 32, No. 2, April 2023 (© 2023)
https://doi.org/10.1007/s11053-022-10152-6

Original Paper

Dynamic Characteristics of Coal under Triaxial Constraints Based on the Split–Hopkinson Pressure Bar Test System

Zhoujie Gu,[1,2] Rongxi Shen,[1,2,3] Zhentang Liu,[1,2,3] Enlai Zhao,[1,2] Hailiang Chen,[1,2] Zichen Yuan,[1,2] Xiaomeng Chu,[1,2] and Jiawei Tian[1,2]

Received 23 July 2022; accepted 16 December 2022
Published online: 5 January 2023

Deep coals are mostly in a three-dimensional (3D) unequal stress state. In the hope of revealing dynamic characteristics of deep coals under impact load, dynamic failure experiments were performed on coal samples under dynamic load through the triaxial Split–Hopkinson pressure bar test system. In addition, the dynamic characteristics of coal in the multi-axial pre-stress state were analyzed by sampling the signals of incident, reflected and transmitted waves. Moreover, the relationships of dynamic peak strength, macroscopic fracture morphology of coal with axial pressure and confining pressure were explored. The following conclusions were drawn: The 3D pre-stress state exerts an obvious constraint on the dynamic failure of coal. With increase in strain, the dynamic initial stress of coal increases linearly first, and then grows at a reduced rate until the peak strength. After that, the mechanical curve rebounds notably. With increases in vertical force σ_2 and horizontal force σ_3, the dynamic strength of coal increases gradually. Under uniaxial impact, coal is broken into particles or powder, while in 3D pre-stress state, coal presents macroscopic fracturing. The dynamic strength factors of coal vary obviously with the increase of confining pressure. The research results can provide reference for the study on dynamic characteristics of coal under multi-axial constraints and for the prevention and control of dynamic disasters induced by dynamic loads in deep coals.

KEY WORDS: Hopkinson pressure bar, True triaxial, Stress–strain, Dynamic strength, Fracture morphology.

INTRODUCTION

With increase in mining depth, crustal stress increases gradually and rock burst occurs in mines more often. Consequently, coal rock dynamic disasters have become a research hot spot in coal rock dynamics (Hast 1969; He et al., 2015; Li et al., 2017). Many studies have shown that, different from the mechanical properties of shallow coal, deep coal under high stress is mostly in a three-dimensional (3D) unequal stress state (Seager 1964; Lee 1976; McGarr and Gay 1978; Si et al., 2020). During coal seam mining, coal is affected by blasting stress wave and seismic wave caused by roof instability and collapse, and such effects pose dynamic disturbance to coal rock under high static load. The above two effects jointly constitute the mechanical environment of deep coal rock under coupled static–dynamic loads (Jamison et al., 2010; Mudau et al., 2016; Fan et al., 2018; Liang et al., 2020). Considering the present exploitation status of deep coal and the

[1]Key Laboratory of Gas and Fire Control for Coal Mines, Ministry of Education, China University of Mining and Technology, Xuzhou 221116, Jiangsu, China.
[2]School of Safety Engineering, China University of Mining and Technology, Xuzhou 221116, Jiangsu, China.
[3]To whom correspondence should be addressed; e-mail: shenrongxi@126.com, keenliuandq@163.com

force conditions of coal in underground engineering, studying the dynamic characteristics of coal under multi-axial pre-stress is of great significance for the prevention of deep coal rock dynamic disasters.

To reveal the mechanical properties and fracture behavior of coal rock under constraint conditions, many scholars (e.g., Sato et al., 1981; Yin et al., 2015; Feng et al., 2017; Kong et al., 2018) have performed extensive static triaxial compression experiments. Mogi (1971) investigated accurately the mechanical behavior of rock under three unequal principal stresses with the aid of a self-made triaxial test device. It was concluded that the strength of rock depends on the intermediate principal stress σ_2. Liu et al. (2019a) explored the mechanical properties and failure behavior of dried and saturated coal samples under true triaxial loading stress, and pointed out the influence of water weakening and intermediate stress on the mechanical properties and failure behavior of coal. Lu et al. (2020a; 2020b) studied the strength and failure characteristics of coal under different loading paths by a true triaxial testing machine and found that the peak stress strength of coal increases first and then decreases with increase in intermediate principal stress under the same force σ_3.

Due to the influence of dynamic disturbance on coal rock under high static load, the Split–Hopkinson pressure bar (SHPB) test has been widely used to study the dynamic characteristics of coal rock (Green et al., 1968). Many scholars have designed uniaxial SHPB dynamic experiments and found that the dynamic strength of coal rock is affected significantly by the variation of impact velocity (Green et al., 1968; Liu et al., 2020a, 2020b, 2020c; Feng et al., 2022). Liu et al. (2020a, 2020b, 2020c) performed impact tests on granite under different loading rates with the aid of SHPB system and researched the response characteristics of acoustic emission of rock during dynamic failure. Xiao et al. (2009) tested the dynamic compressive strength, peak strain, residual strength and secant stiffness and other parameters of concrete through experiments. Li et al. (2009a, 2009b) made a comparative analysis of the mechanical properties, strength differences and macroscopic failure modes of rocks under static and dynamic loads by static and dynamic load impact experiments. Li et al. (2011) studied the propagation and reflection characteristics of coal rock stress wave by SHPB impact experiments. Li et al. (2018) analyzed the dynamic characteristics, deformation and micro-structure of sandstone under multiple impacts via SHPB impact experiments driven by the dropping hammer.

Considering the influences of axial pressure and confining pressure on the dynamic characteristics of coal rock, a triaxial SHPB test device was developed. Gong et al. (2019) studied the effect of dynamic properties of sandstone under triaxial compression, explored the correlation between failure mode and stress curve of sandstone samples, and analyzed the dynamic Mohr–Coulomb criterion and dynamic Hoek–Brown criterion under confining pressure. Jin et al. (2013, 2020) conducted cyclic impact experiments on rocks and investigated the change law of dynamic strength and stress wave of rocks during cyclic impact. Kong et al. (2021a, 2021b) designed the dynamic experiments on gas-containing coal to study its dynamic characteristics, established its dynamic constitutive equation, and analyzed the influence of different axial static load, confining pressure, impact velocity and methane pressure on the dynamic mechanical properties of coal samples.

In deep mining, most coal rock is subjected to 3D unequal stress. In view of this fact, Xu et al. (2020) tested and analyzed the dynamic mechanical characteristics of concrete with the aid of a self-made true triaxial SHPB device. Liu et al. (2019a, 2020b, 2020c) studied the dynamic mechanics and fracture behavior of sandstone and concrete under changing 3D pre-stress with a self-developed triaxial SHPB device. Xie et al. (2021) developed a new 3D rock dynamic test based on true triaxial electromagnetic SHPB system, which can realize triaxial 3D dynamic impact experiments. You et al. (2021, 2022) carried out true triaxial SHPB impact experiment to study the law of mechanical strength of rock under the change of pre-stress σ_1, σ_2 and strain rate. All the above-cited studies concluded that the dynamic strength of rock or concrete decreases with increasing axial pre-stress σ_1 along the impact direction, while it increases with increase in lateral pre-stresses σ_2 and σ_3. The rock or concrete under high pre-stress mainly suffers from shear failure. Liu and Zhao (2021) and Luo et al. (2022) conducted repeated impact tests on rocks under true triaxial pre-stress respectively, and analyzed that the mechanical strength of rocks decreases gradually with increase of impact times, the absorbed energy presents a cumulative effect, and the dissipated energy increases gradually. Compared with high-strength rock or concrete, the surface of coal is smooth without fine cracks. The material of coal

sample itself is quite different from that of rock and concrete. There may be derived cracks on the surface of coal sample, and the interior is sparse and porous. The mechanical evolution law and failure behavior of coal under dynamic load may be significantly different from that of rock, and so it is of great significance to carry out coal body dynamics experiment.

Although extensive uniaxial and conventional triaxial SHPB experiments have been performed to explore the dynamic characteristics of coal, true triaxial SHPB dynamic experiments are rarely reported. Therefore, true triaxial SHPB dynamic experiments on the dynamic mechanical characteristics of coal are conducive to the in-depth study on the influence of 3D ground stress on coal rock dynamic disasters. In this research, the triaxial SHPB system was employed to carry out the experiment and to collect experimental data. The relationships of the dynamic mechanical curve, peak strength, strain and fracture morphology of coal mass with axial pressure and confining pressure were explored and discussed. The research results can provide an experimental and theoretical basis for the prevention and control of disasters induced by coal rock disturbance under an unequal stress state.

EXPERIMENT

Experimental Sample Preparation

In the experiment, coal samples which exhibited relatively good integrity and homogeneity were selected from a mining area in Shaanxi Province, China. The experimental coal samples were processed according to the performance test requirements of coal rock mechanics routine tests. For the true triaxial dynamic load impact tests, all samples were uniformly processed into cubes of 47 mm × 47 mm × 47 mm (Fig. 1). Some parameters of the samples were as follows: static compressive strength ~ 28.8 MPa, elastic modulus 2.2 GPa, density 1.3 g/cm^3, and wave velocity 1.9 km/s.

Experimental System

The experimental system (Fig. 2) consisted mainly of the following subsystems: the true triaxial pressure operating system, the true triaxial main body system, the data acquisition system, the main part of pressure bar and the operating table system. The true triaxial pressure operating system was made up of a pressure operating display and a loading controller. The true triaxial main body system included axial, horizontal and vertical hydraulic cylinders that can apply 3D pre-static loads, namely axial force σ_1, vertical force σ_2 and horizontal force σ_3. The data acquisition system had a superdynamic strain gauge, strain gauges, a strain connection box and a speedometer. The main part of pressure bar comprised a barrel, an impact bar (commonly known as bullet), an incident bar, a transmission bar and corresponding pressure devices. The operating table system was composed of a power switch, a data acquisition interface and a launcher.

The bullet, incident and transmission bars of the experimental system, which were 0.4 m, 5 m and 3 m in length, respectively, were made of 30Crmosini2a steel; besides, the elastic modulus was 210 GPa, the longitudinal wave propagation velocity 5100 m/s, and the bar diameter 100 mm. The strain gauges were affixed to the middle of the incident and transmission bars in a symmetrical way in order to collect the pulse signal generated by the impact.

Experimental Loading Path

Pre-stress conditions mainly included uniaxial ($\sigma_1 > \sigma_2 = \sigma_3 = 0$), biaxial ($\sigma_1 \geq \sigma_2 > \sigma_3 = 0$) and triaxial ($\sigma_1 \geq \sigma_2 \geq \sigma_3 \neq 0$) states. Static load pre-stress was applied to the cubic samples by axial, horizontal and vertical hydraulic cylinders. Dynamic load was provided by bullet emission so as to realize triaxial static–dynamic coupled loads and perform triaxial impact experiments.

In this study, under the same impact velocity, dynamic impact experiments were carried out on coal samples under different pre-stress states. The pre-stress loading path is shown in Figure 3. The axial and confining pressures of the samples were increased to the stress state of $\sigma_1 \geq \sigma_2 \geq \sigma_3$ at a low loading rate with the aid of the hydraulic cylinder, and then the dynamic load was applied along the direction of σ_1 to complete the dynamic load impact experiments.

The uniaxial and true triaxial SHPB dynamic characteristics of coal were explored by setting different confining pressure gradients. The setting of pre-static load parameters of coal samples is exhibited in Table 1. Many experiments were performed according to the experimental schemes and then

Figure 1. Experimental coal samples.

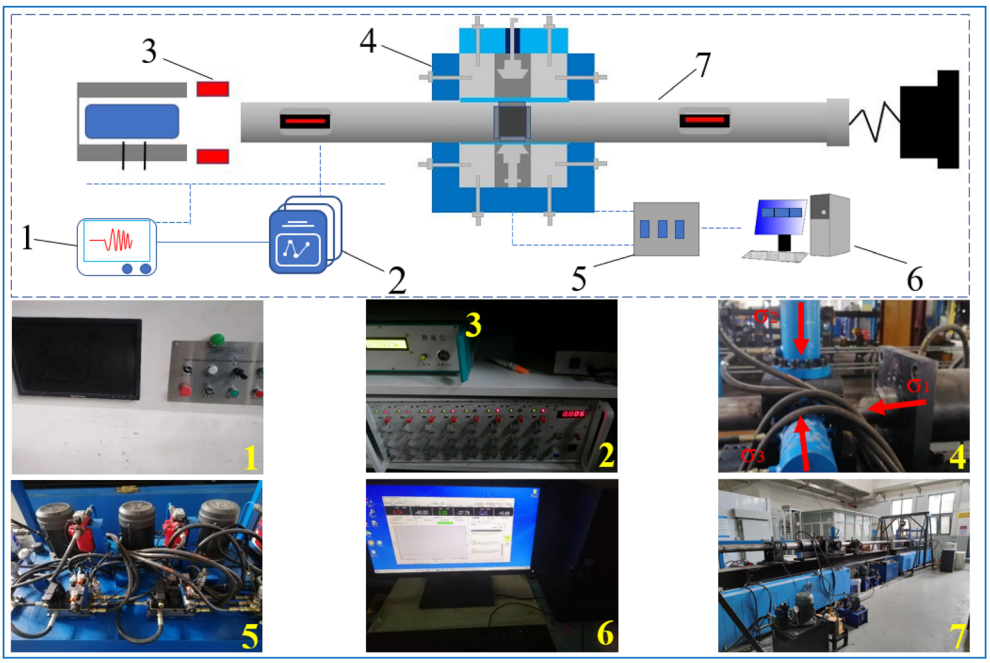

Figure 2. Diagram of the experimental system. 1 = launch system; 2 = super strain gauge; 3 = speedometer; 4 = triaxial cavity; 5 = three = way oil pump; 6 = pre = stress loading; 7 = main part.

representative coal samples were selected for data analysis. The six coal samples selected were denoted as T1–T6.

Experimental Procedure and Principle

First, the coal sample was put into the test chamber and subjected to preset stress in the axial, vertical and horizontal directions by the loading system. The preparation for the experiment included turning on the air compressor to enable the launcher to reach the corresponding pressure and setting the infrared speedometer and superdynamic strain system. Then, the pneumatic device launched the bullet and impacted the incident bar. The infrared speedometer was triggered automatically to measure the impact velocity. The superdynamic strain gauge collected the stress wave signals during the experiment with the aid of the strain gauges. In the uni-

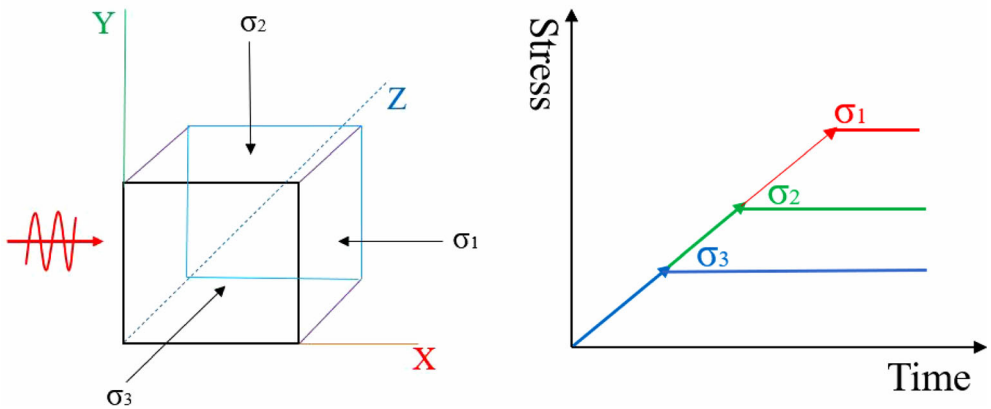

Figure 3. Experimental loading directions and paths.

Table 1. Settings of experimental schemes

Number	Static load pre-stress		
	Axial stress σ_1/MPa	Vertical stress σ_2/MPa	Horizontal stress σ_3/MPa
1	8	0	0
2	8	0 +	0 +
3	8	2	2
4	8	4	2
5	8	6	2
6	8	6	4

axial impact experiment, the high-speed camera (14,000 frames) was started to shoot and observe the morphological changes of coal samples during the impact. After the experiment, the tester saved the data and 3D confining pressure of the sample was relieved at a low speed. Afterwards, the tester took out the sample from the chamber and examined its morphology. Subsequently, the next group of experiment was performed.

As shown in Figure 4, the stress wave propagates in the incident bar upon the strike of bullet. When the incident wave reaches the contact interface between the incident bar and the sample, one part of the incident wave is reflected, and the other part propagates in the sample. When the incident wave reaches the contact interface between the sample and the transmission bar, the reflection and transmission occur again. The stress wave propagates in the incident bar, the sample and the transmission bar through multiple reflections and transmissions, forming the incident wave $\varepsilon_{i,}$ the reflected wave ε_r and the transmission wave ε_t.

Since the pre-stress was loaded in advance in three directions of X/Y/Z in the specimen, the impact was carried out along the axial X direction, the interpretation of dynamic strain data obtained in the true triaxial impact tests still followed the one-dimensional (1D) elastic wave propagation theory (Liu et al. 2019; You et al. 2021; Luo et al, 2022). The test principle is the same as that of 1D dynamic load tests; both are based on the 1D stress wave assumption and the stress homogenization assumption (Liu et al. 2019; Xie et al. 2021).

Therefore, when processing stress wave signals, the first incident wave, reflected wave and transmission wave were selected for calculation by the method of three-wave separation (Fig. 5). Figure 5 shows the stress wave curve under different pre-stress. When the stress wave propagates to the coal sample, abundant stress waves are reflected, leaving only a small part of the stress wave transmitting energy through the sample. For all the coal samples, the form of incident wave is relatively stable, and the amplitudes of reflected wave and transmission wave

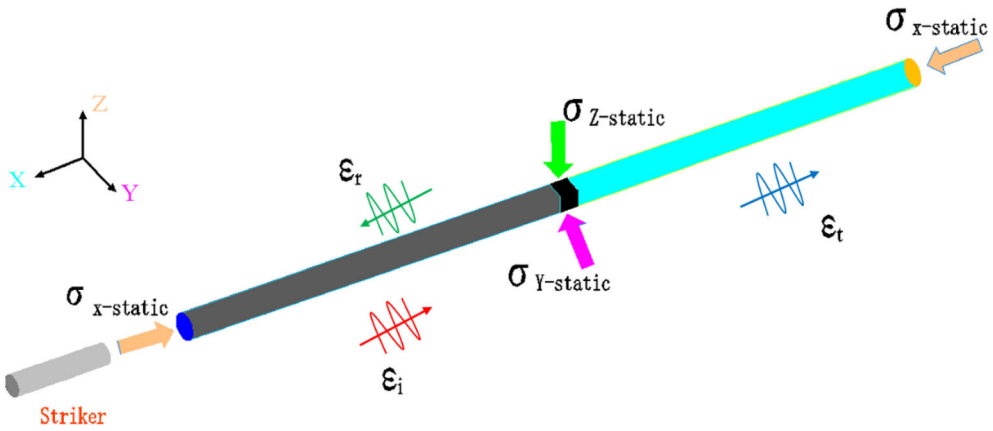

Figure 4. Schematic diagram of axial stress wave propagation.

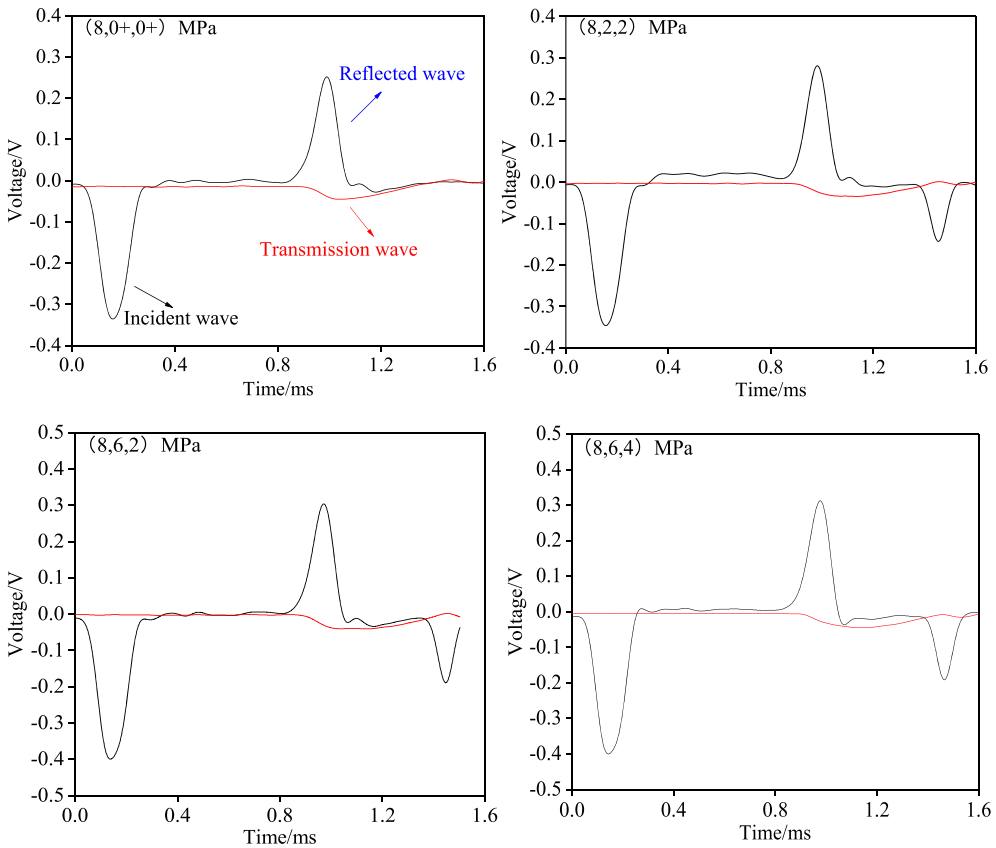

Figure 5. Stress wave waveforms collected.

are smaller than that of incident wave. Based on the 1D stress wave assumption and the stress homogenization assumption, the average strain rate, strain and stress of the sample can be derived (You et al., 2021; Luo et al., 2022), thus:

$$\dot{\varepsilon}(t) = \frac{C}{L_0}[\varepsilon_i(t) - \varepsilon_r(t) - \varepsilon_t(t)] \quad (1)$$

$$\varepsilon(t) = -\frac{C}{L_0}\int_0^t [\varepsilon_r(t) + \varepsilon_t(t) - \varepsilon_i(t)]dt \quad (2)$$

$$\sigma(t) = \frac{A}{2A_0}E[\varepsilon_i(t) + \varepsilon_r(t) + \varepsilon_t(t)] \quad (3)$$

where C is the propagation velocity of stress wave in elastic bar, L_0 is the sample length, E is the elastic modulus of the elastic bar, A is the cross-sectional area of the elastic bar, A_0 is the cross-sectional area of the sample, and t is the duration of stress wave pulse.

As shown in Figure 6, the strain under different loading conditions changed regularly with time. The results showed that the reflected strain was larger than the transmission strain, indicating that most of the incident waves were reflected after impact. The reflected strain and transmission strain increased with increase in confining pressure, and the amplitude growth rate of the transmission strain was more significant. This is because, with the gradual increase of pre-stress on the coal sample, the sample became more compact, improved the compactness of the coal sample, and promoted more transmission waves to pass through.

Figure 7 exhibits the stress balance between the two ends of the coal sample. For example, under the pre-stress [(8, 0 + , 0 + MPa) and (8, 6, 4 MPa)], the curve of the sum of incident strain and reflected strain (Int + Re) almost completely coincided with the transmitted strain curve, indicating that the sample had realized the stress balance in the process of dynamic compression, with its left and right ends subjected to equal stress.

ANALYSIS ON EXPERIMENTAL RESULTS

SHPB Dynamic Curve Characteristics of Coal under Multi-Axial Constraints

The dynamic curves are shown in Figure 8. Curve variation of T1 coal sample ($\sigma_1 = 8$, $\sigma_2 = \sigma_3 = 0$): In the initial compaction stage oa, there were a lot of micro-cracks in the coal. In the early stage of impact loading, the micro-cracks closed gradually under compressive stress; the stress–strain curve of ab stage soared linearly, representing the linear elastic stage during coal failure. Then, entered the bc stage of plastic deformation, with increase in strain, the increase rate of stress slightly slowed down, representing the stable deformation stage; the pores within the coal sample began to connect and developed into cracks. As the newly generated cracks and the original cracks continued to develop, the strain continued to increase and the stress reached the peak (point A(c)). The ce stage was the failure process of coal, among which cd stage had a stress plateau stage, and the stress was almost constant with increase in strain. This is because the internal and surface failure cracks of coal samples continued to expand, but the whole sample was not completely open to fragmentation and splash. In the first unloading stage of de, with continuous increase in strain, the stress decreased slightly, indicating that the coal body decreased gradually after experiencing the peak stress, and the overall damage of the coal sample was more significant, and the structural plane was damaged significantly (Liu et al., 2021). The ef is the second unloading stage, where the stress continued to decrease and the strain decreased gradually due to rebound effect (Li et al. 2018).

Curve variation of T3 coal sample ($\sigma_1 = 8$, $\sigma_2 = \sigma_3 = 2$): the stress varied rapidly with strain in the initial stage. The stress curve of the coal sample almost escaped the compaction stage, which is different from that of conventional coal rock (Shen et al., 2020; Li et al. 2021; Ding et al., 2022). With increase in strain, the stress growth decelerated slightly, and the decelerating rate was lower than that of T1 curve. As the strain continued to increase, the stress reached the peak, which means the coal entered the unloading stage. After the stress peak, the strain declined slowly.

Due to the existence of confining pressure, the peak stress of T3 was higher than that of T2 and T1. This suggests that compared with the constraint of uniaxial force σ_1, the applied vertical force σ_2 and horizontal force σ_3 promoted the dynamic strength of coal. 3D pre-stress exerts a significant constraint on the coal sample (Liu et al., 2019, 2020c) and greatly enhances its dynamic strength.

SHPB Dynamic Curve Characteristics of Coal in a 3D Pre-stress State

Figure 9 exhibits the dynamic stress–strain curves of coal samples under varying 3D pre-stresses ($\sigma_1 > \sigma_2 > \sigma_3 > 0$). Under constant impact velocity, the axial, vertical and horizontal pre-stresses in-

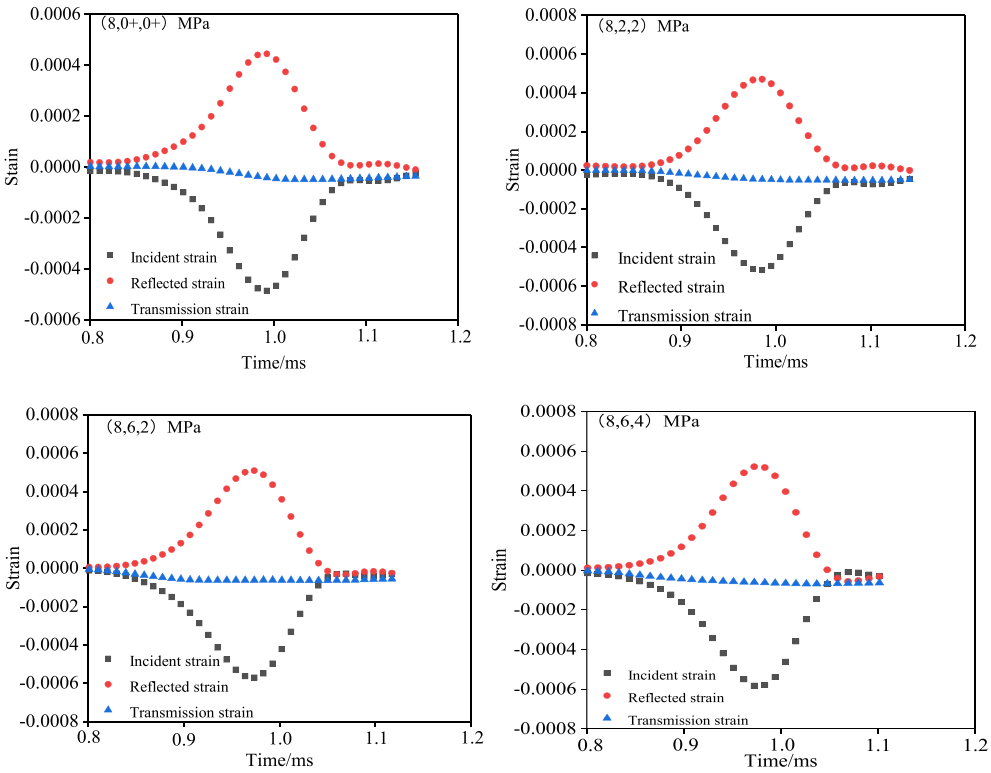

Figure 6. Strain evolution with time under different loading conditions.

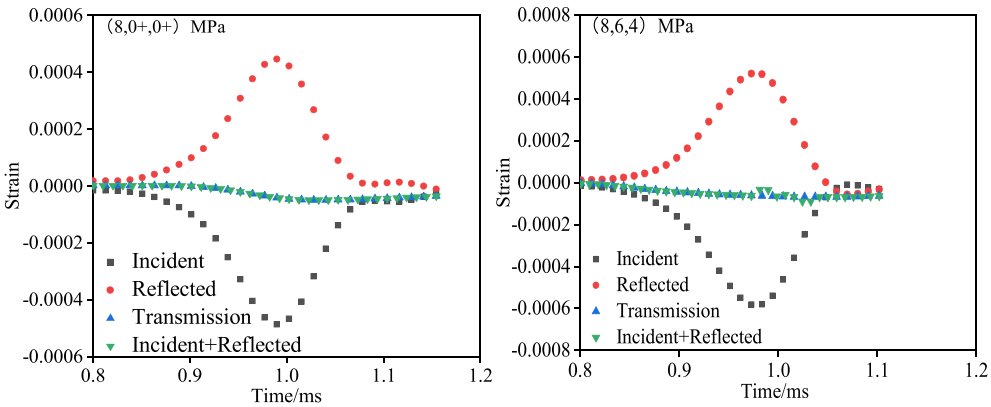

Figure 7. Dynamic stress balance check.

creased in turn based on the 3D static load stress (8, 2, 2 MPa). In this case, the following stress–strain curve characteristics under a high confining pressure were observed: The initial dynamic stress of coal surged, and then the increase slowed down until the peak stress stage. The strength of coal plunged after the initial fracture, and T2–T6 curves varied in basically the same trend. Under the 3D stress constraints, the stress of coal dropped rapidly after the peak stress, and the stress curve presented a rebound. This research conclusion has similarities with previous researched on the dynamic characteristics of rock or concrete under triaxial unequal pre-stress (Cui et al. 2019; Liu et al. 2019, 2020c).

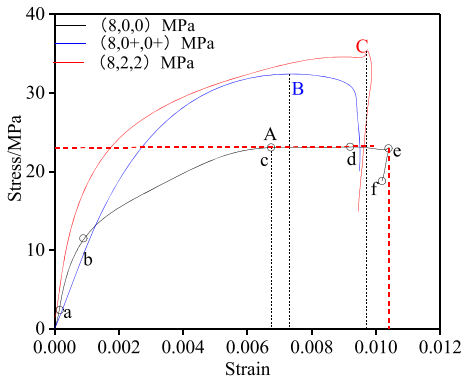

Figure 8. Multi-axial SHPB dynamic curves.

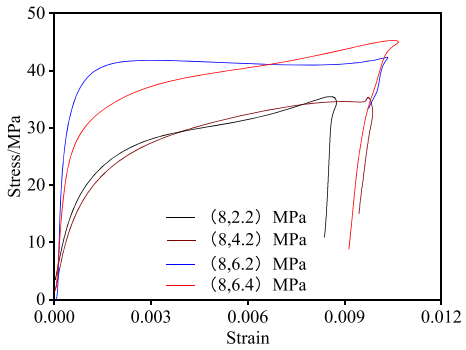

Figure 9. True triaxial SHPB dynamic curves.

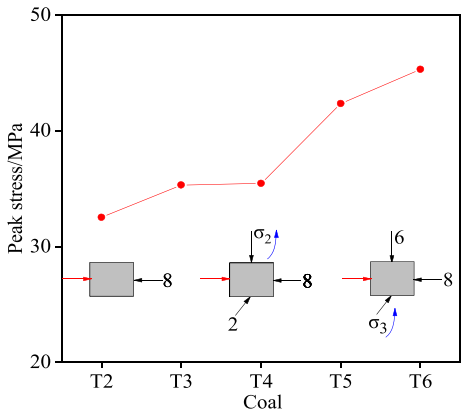

Figure 10. Variations of peak stress of coal samples under varying 3D pre-stresses.

Figure 10 shows the variations of peak stress and strain of coal samples under varying 3D pre-stresses. With increase in 3D pre-stress, the dynamic peak strength rose gradually. When the preset confining pressure was (8, 6, 4 MPa), the maximum of dynamic strength occurred. A combination of Figures 9 and 10 fully verifies the constraints of 3D unequal pre-stress on coal samples under impact in that the dynamic strength increased significantly.

Fracture Characteristics of Coal Samples

The process of coal crushing under uniaxial impact captured by a high-speed camera is illustrated in Figure 11. As shown in Figure 11, when the incident bar just contacted the coal sample, no obvious crack occurred on the surface of the coal sample. At 71 μs, a visible crack occurred in the lower left corner of the sample, which may be caused by the uneven contact stress between the bar and the coal sample (Cai et al., 2020). At 143 μs, a crack occurred along the axial direction of the bar, which may have resulted from the instantaneous impact of the incident bar vibration disturbance on the coal sample. Then, at 286 μs, the axial crack propagated along the vertical direction. After 571 μs, the crack continued to expand along the vertical direction until the sample was completely broken into particles.

The characteristics of coal sample failure under the same impact velocity are exhibited in Figure 12. Under uniaxial impact, the coal sample was crushed into powder, showing a high degree of fragmentation. Under (8, 2, 2 MPa), the coal generated cracks and its surface fell off. The surface cracks constituted combined failure of tension and compression-shear. Compared with only static load axial stress, 3D stress exerted a significant constraint on the dynamic failure of coal, causing a low degree of fragmentation.

From Figure 13, under (8, 4, 2 MPa), the coal sample generated cracks similar to that under (8, 2, 2 MPa), thus mainly underwent shear failure accompanied by tensile failure. As the vertical static load stress increased from 2 to 6 MPa, the integrity of the coal sample was gradually intact after destruction. The overall failure was that the cracks on each action surface were connected to form a macro-fracture zone.

Under high confining pressure of (8, 6, 4 MPa), the coal sample had a low degree of fragmentation, and the cracks were mainly compression-shear failure, which resembled the fracture morphology of rock and concrete reported in relevant literature (Liu et al., 2019). Figure 13 reveals that the lateral

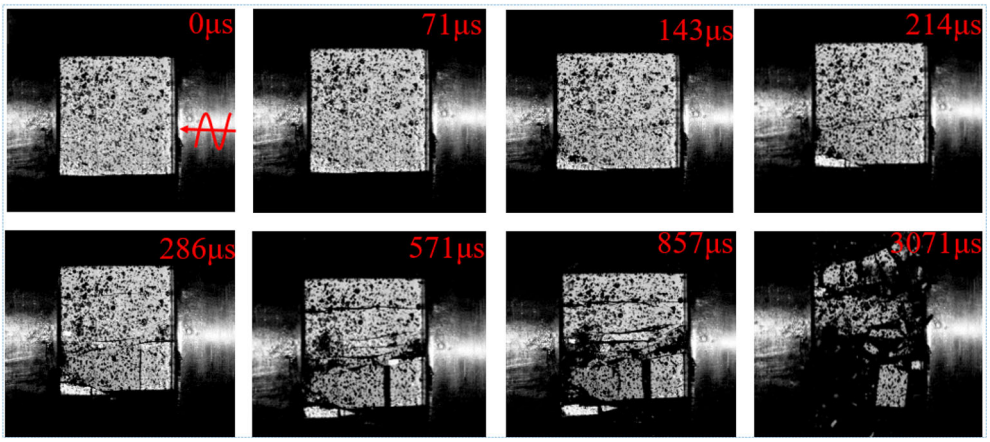

Figure 11. Fracture morphology evolutions of the coal sample under uniaxial impact.

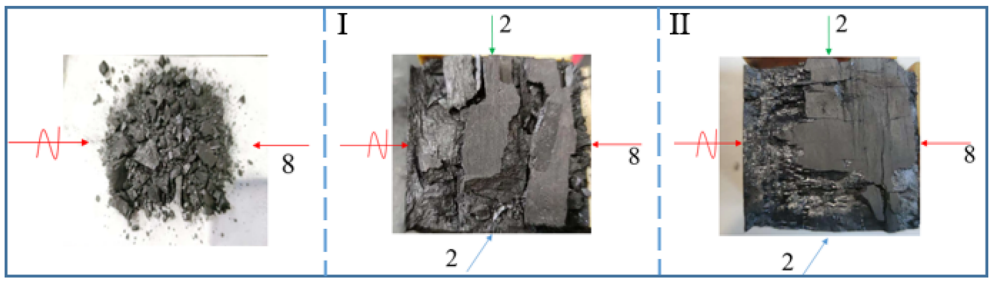

Figure 12. Macroscopic morphology of the coal sample failure under uniaxial and triaxial impact.

constraint pressure can inhibit crack propagation (Chen and Ravichandran 1997), and the multi-stress state or the lateral constraint helped enhance the strength of coal.

DISCUSSION

Influence of Confining Pressure on Dynamic Characteristics of Coal

Based on the above-discussed experimental research, under triaxial precompression, the dynamic strength of coal changed significantly due to the existence of 3D pre-stress. Under the lateral constraint, the stress situation of the coal sample differed from the mechanical behavior of that under conventional dynamic triaxial compression.

Figure 14a displays the conventional triaxial stress of coal sample. To achieve such a stress state, the coal sample was generally processed into the shape of a round cake shape and was uniformly stressed in the vertical direction in a fully enclosed state created by the loading device of confining pressure ($\sigma_1 > \sigma_2 = \sigma_3 > 0$) (Yin et al., 2012; Gong et al., 2019; Li et al. 2019; Kong et al., 2021b; Ma et al., 2021). Figure 14b illustrates the true triaxial stress diagram of a standard cubic coal sample subject to static load from three directions. The lateral confining pressure on the sample was σ_2 and σ_3 ($\sigma_1 \geq \sigma_2 \geq \sigma_3 \neq 0$). As disclosed through a comparison of the two samples, the one under the combined impact of dynamic–static loads presents notably more complex stress conditions and types compared with the one under conventional triaxial stress.

As can be seen from Figures 8 and 9, the characteristics of dynamic failure stress–strain curves of the T1–T3 coal samples (under uniaxial and true triaxial impacts) and T2–T6 coal samples (under variable confining pressure) were as follows: The stress surged in the initial stage, then grew at a

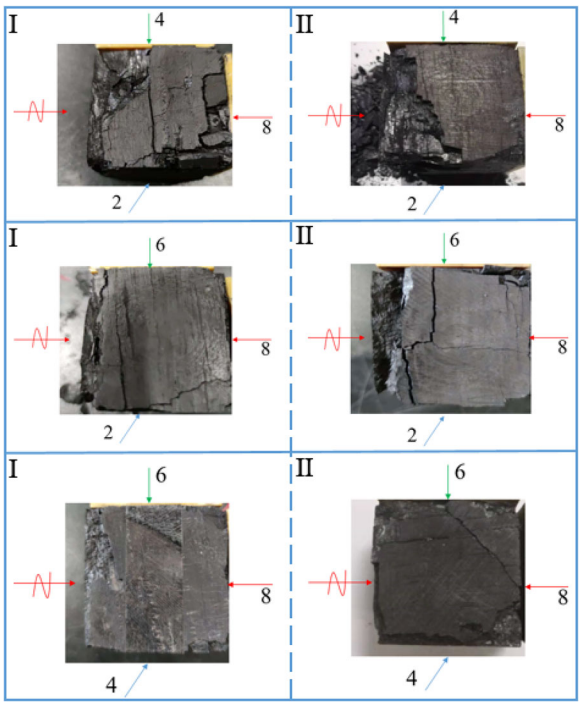

Figure 13. Macroscopic morphology of coal sample failure under true triaxial impact.

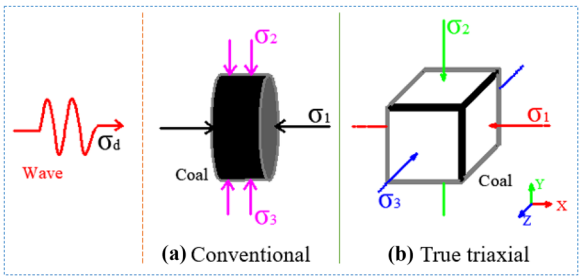

Figure 14. 3D stress diagram of coal samples.

slightly reduced rate, and finally reached the peak stress. In the whole process, the stress–strain curves almost escaped the compaction stage. According to analysis, because of the short dynamic loading duration caused by pre-stress constraint and impact load, coal became compacted and entered the elastic deformation stage quickly. As a result, the compaction stage was not significant in the stress–strain curve of the coal sample.

It can be seen from Figure 10 that with the gradual increase of the 3D pre-stress, the dynamic strength of coal was enhanced remarkably, which verifies that the dynamic strength of coal was constrained by axial pressure and confining pressure. The test results demonstrate that under a certain impact velocity, the increase of coal strength depended on the confining pressure constraint condition.

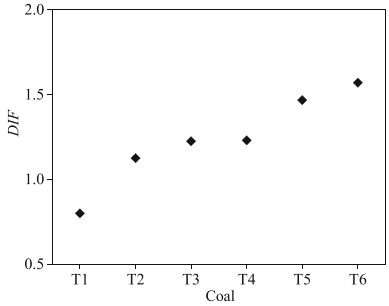

Figure 15. Variation law of DIF.

Combined with the analysis on coal crushing morphology in Figures 11, 12 and 13, the coal sample was broken significantly and even impacted into fragments or even powders in the dynamic uniaxial compression test, resulting in the continuous increase of post-peak strain. However, under 3D high pre-stress, the coal sample was approximately intact with only slight deformation or micro-cracks. The fracture behavior of coal was mainly determined by the constraint conditions.

Analysis on Dynamic Strength Factor

Dynamic strength factor (DIF) is an important parameter for studying the relationship between dynamic compressive strength and strain rate of materials such as concrete (Bailly et al., 2011; Hao and Hao 2014; Cui et al., 2018; Liu et al., 2020c). Considering that coal and concrete can be used as similar materials, we calculated the DIF of coal as:

$$\mathrm{DIF} = \sigma_{\mathrm{d}}/\sigma_{\mathrm{c}} \tag{4}$$

where σ_{d} is the dynamic compressive strength (MPa), and σ_{c} is the static compressive strength (MPa).

The relationships of DIFs of the coal samples under varying pre-stresses are reflected in Figure 15. Under the same impact velocity, the DIF of coal sample under uniaxial impact was relatively low, while that of coal sample under triaxial impact rose with increase in confining pressure. It is concluded that the pre-stress had a great influence on the dy-

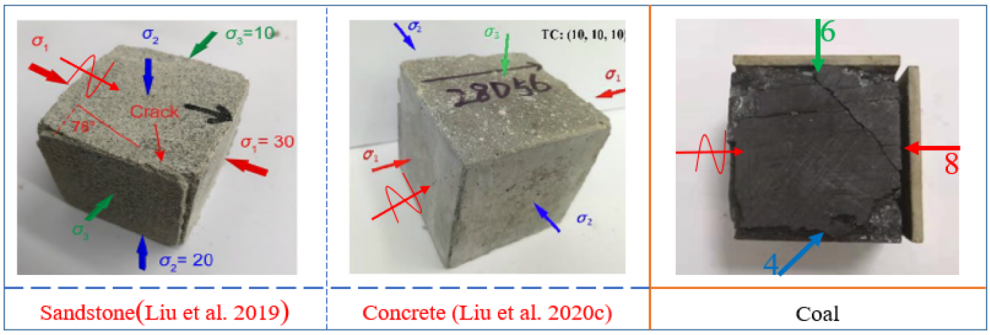

Figure 16. Fracture morphologies of different materials after impact.

namic compressive strength of coal sample. Under triaxial impact, the coal sample was more constrained than the one under uniaxial impact, and thereby its DIF was also larger.

True triaxial SHPB tests are performed on rock and concrete under a higher confining pressure (static load pre-stress up to 30 MPa) and at a higher impact velocity (velocity above 10 m/s) (Fig. 16 [Liu et al., 2019b, 2020c]). The DIF of concrete was estimated to be about 1.5–3 (Liu et al., 2020c). In this experiment, the DIFs of the coal samples were about 0.8–1.6. The significant differences in DIF may be caused by many factors such as static compressive strength, 3D pre-stress, impact velocity and material difference in different experiments.

In this experiment, by setting different confining pressures, the variations of dynamic strength and peak strain of coal under true triaxial dynamic and static load combination were studied and analyzed preliminarily, and the macroscopic failure morphology of coal under high confining pressure was analyzed. Different from rock and concrete, coal contains many primary pores and cracks on the surface, and it features relatively higher dispersion and lower compressive strength under static load. Besides, during loading, coal breaks easily and corresponds to a more complex dynamic mechanism.

Dynamic Characteristics under 3D Stress Evolution

As shown in Figure 17, for the original coal seam, the coal stratum was in 3D stress balance before tunneling. With the excavation of underground roadways, the original stress state of coal and rock strata was broken and the stress was redistributed. The stress state of roadway surrounding

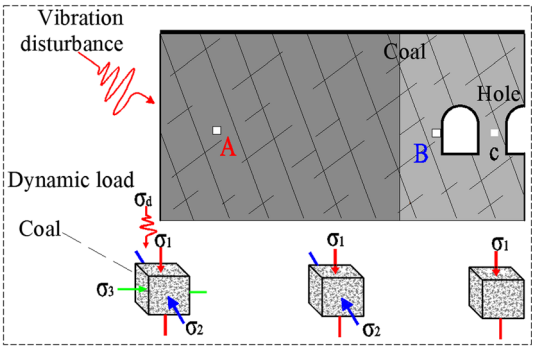

Figure 17. Stress evolution of deep coal body.

rock changed from three-way stress state to two-way stress state. The stress of coal seam changed from two-way compression to one-way compression. With the provision of dynamic load stress, a 3D stress state of dynamic and static load combination was formed.

The use of the developed true triaxial SHPB device will provide an important experimental means for studying the influence of 3D stress evolution of coal and rock on rockburst in the future. The fracture morphology analysis of the sample after the experiment also provides a theoretical basis for the future study of its fracture mechanism.

The experimental results show that the dynamic compressive strength increased obviously when the 3D pre-stress of coal seam was large. Therefore, when the coal bearing stress is large and the 3D stress difference is large, corresponding measures need to be taken to improve the surrounding rock stress environment to make it close to the 3D equal stress, so as to slow down the coal seam damage under dynamic load impact. The research and

development of the true triaxial SHPB device and the related research results have reference significance for the mechanism and prevention of coal rock impact failure.

CONCLUSIONS

In this study, the dynamic mechanical properties of coal samples were studied with the aid of the true triaxial SHPB system. The device can apply 3D pre-stress on coal samples ($\sigma_1 \geq \sigma_2 \geq \sigma_3 \geq 0$) and dynamic load along σ_1 direction. Besides, the dynamic mechanical properties of coal under multi-axis constraints were analyzed by collecting stress wave signals, which provides an experimental basis for studying the disaster mechanism of coal rock burst under 3D ground stress.

Through the true triaxial SHPB impact experiment, the dynamic characteristics of coal samples were analyzed. The dynamic stress soared in the initial stage, then the stress variation slowed down slightly until the peak strength; subsequently, it rebounded significantly.

Compared with the coal sample in the uniaxial state, the one in the 3D pre-stress state had a higher dynamic strength. This reflects the constraint effect of confining pressure on the dynamic failure of the coal sample. With increases in the vertical force σ_2 and horizontal force σ_3, the dynamic strength of coal sample continued to increase. The dynamic strength factor of coal jumped significantly with increase in confining pressure.

Under uniaxial impact, coal was broken into particles or powder, while in 3D pre-stress state, coal presented a low degree of fragmentation and slight macroscopic fracturing. The failure mode of coal also reflects the constraint applied by the confining pressure. The research results can provide reference for the research on the dynamic characteristics of coal under multi-axial constraints and for the prevention and control of dynamic disasters induced by dynamic load in deep coals.

ACKNOWLEDGMENTS

We gratefully acknowledge the financial support for this work provided by the National Natural Science Foundation of China (52074276), the Fundamental Research Funds for the Central Universities (2019XKQYMS55). We thank reviewers for their comments and suggestions to improve the manuscripts.

DECLARATIONS

Conflict of Interest The authors declare that there is no conflict of interest regarding the publication of this paper.

REFERENCES

Bailly, P., Delvare, F., Vial, J., Hanus, J. L., Biessy, M., & Picart, D. (2011). Dynamic behavior of an aggregate material at simultaneous high pressure and strain rate: SHPB triaxial tests. *International Journal of Impact Engineering, 2–3*, 73–84.

Cai, X., Zhou, Z. L., & Du, X. M. (2020). Water-induced variations in dynamic behavior and failure characteristics of sandstone subjected to simulated geo-stress. *International Journal of Rock Mechanics and Mining Sciences, 130*, 104339.

Chen, W., & Ravichandran, G. (1997). Dynamic compressive failure of a glass ceramic under lateral confinement. *Journal of the Mechanics & Physics of Solids, 45*(8), 177–182.

Cui, J., Hao, H., Shi, Y. C. (2018). Numerical study of the influences of pressure confinement on high-speed impact tests of dynamic material properties of concrete. *Construction and Building Materials*, 839–849.

Cui, J., Hao, H., Shi, Y. C., Zhang, X. H., & Huan, S. (2019). Volumetric properties of concrete under true triaxial dynamic compressive loadings. *Journal of Materials in Civil Engineering, 31*(7), 04019126.

Ding, Z., Feng, X., Wang, E., Wei, Q., Zhao, X., & Hu, Q. (2022). Acoustic emission response and evolution of precracked coal in the meta-instability stage under graded loading. *Engineering Geology, 312*, 106930.

Fan, C., Kefu, Y. U., Meng, Q., & Zeng, W. (2018). Review of the SHPB in rock dynamics research[J]. *Soil Engineering and Foundation., 005*, 032. (in Chinese).

Feng, X., Ding, Z., Ju, Y., Zhang, Q., & Ali, M. (2022). ''Double Peak'' of dynamic strengths and acoustic emission responses of coal masses under dynamic loading. *Natural Resources Research, 31*(3), 1705–1720.

Feng, X. T., Zhang, X. W., Yang, C. X., Kong, R., Liu, X. Y., & Peng, S. (2017). Evaluation and reduction of the end friction effect in true triaxial tests on hard rocks. *International Journal of Rock Mechanics and Mining Sciences, 97*, 144–148.

Gong, F. Q., Si, X. F., Li, X. B., & Wang, S. Y. (2019). Dynamic triaxial compression tests on sandstone at high strain rates and low confining pressures with split Hopkinson pressure bar. *International Journal of Rock Mechanics and Mining Sciences, 113*, 211–219.

Green, S., Perkins, R. (1968). Uniaxial compression tests at varying strain rates on three geologic materials. In: *The 10th US symposium on rock mechanics (USRMS), American Rock Mechanics Association*.

Hao, Y. F., & Hao, H. (2014). Influence of the concrete DIF model on the numerical predictions of RC wall responses to blast loadings. *Engineering Structures, 73*, 24–38.

Hast, N. (1969). The state of stress in the upper part of the earth's crust. *Tectonophysics, 2*(1), 5–17.

He, M., Sousa, L. E., Miranda, T., & Zhu, G. (2015). Rockburst laboratory tests database–application of data mining techniques. *Engineering Geology, 185*, 116–130.

Jamison., D. B., & Cook, N. G. W. (2010). *Analysis of measured values for the state of stress in the earth's crust*. American Elsevier Pub. Co.

Jin, J. F., Li, X. B., Chang, J. R., Tao, W., & Qiu, C. (2013). Stress-strain curve and stress wave characteristics of rock subjected to cyclic impact loadings. *Explosion and Shock Waves, 33*(6), 613–619. (in Chinese).

Jin, J. F., Yuan, W., Wu, Y., & Guo, Z. Q. (2020). Effects of axial static stress on stress wave propagation in rock considering porosity compaction and damage evolution. *Journal of Central South University, 27*(2), 592–607.

Kong, R., Feng, X. T., Zhang, X. W., & Yang, C. X. (2018). Study on crack initiation and damage stress in sandstone under true triaxial compression. *International Journal of Rock Mechanics and Mining Sciences, 106*, 117–123.

Kong, X. G., Li, S. G., Wang, E. Y., Ji, P. F., Wang, X., Shuang, H. Q., & Zhou, Y. X. (2021b). Dynamics behaviour of gas-bearing coal subjected to SHPB tests. *Composite Structures, 256*(1), 113088.

Kong, X. G., Li, S. G., Wang, E. Y., Wang, X., Zhou, Y. X., Ji, P. F., Shuang, H. Q., Li, S. R., & Wei, Z. Y. (2021a). Experimental and numerical investigations on dynamic mechanical responses and failure process of gas-bearing coal under impact load. *Soil Dynamics and Earthquake Engineering, 142*, 106579.

Lee, F. T., Abel, J. F., Nichols, T. C. (1976). The relation of geology to stress changes caused by underground excavation in crystalline rocks at Idaho Springs, Colorado: A study to understand the effects of geology and rock stresses on mining in complexly deformed anisotropic metas.

Li, E. B., Gao, L., Jiang, X. Q., Duan, J. L., Pu, S. K., & Wang, J. (2019). Analysis of dynamic compression property and energy dissipation of salt rock under three-dimensional pressure. *Environmental Earth Sciences, 78*(14), 388.

Li, S. H., Zhu, W. C., Niu, L. L., Yu, M., & Chen, C. F. (2018). Dynamic characteristics of green sandstone subjected to repetitive impact loading: Phenomena and mechanisms. *Rock Mechanics and Rock Engineering, 51*(6), 1921–1936.

Li, X. B., Gong, F. Q., Tao, M., Dong, L. J., Du, K., Ma, C. D., Zhou, Z. L., & Yin, T. B. (2017). Failure mechanism and coupled static-dynamic loading theory in deep hard rock mining: A review. *Journal of Rock Mechanics and Geotechnical Engineering, 9*, 767–782.

Li, X. L., Liu, Z. T., Feng, X. J., Zhang, H. J., & Feng, J. J. (2021). Effects of acid sulfate and chloride ion on the pore structure and mechanical properties of sandstone under dynamic loading. *Rock Mechanics and Rock Engineering, 51*(12), 6105–6121.

Li, X. B., Zhou, Z. L., Zhao, F. J., Zuo, Y. J., Ma, C. D., Ye, Z. Y., & Hong, L. (2009a). Mechanical properties of rock under coupled static-dynamic loads. *Journal of Rock Mechanics and Geotechnical Engineering, 1*, 41–47.

Li, X. B., Zhou, Z. L., Zhao, F. J., Zuo, Y. J., Ma, C. D., Ye, Z. Y., & Hong, L. (2009b). Mechanical properties of rock under coupled static-dynamic loads. *Journal of Rock Mechanics and Geotechnical Engineering, 1*(1), 41–47.

Li, Y. X., Zhu, Z. M., Li, B. X., Deng, J. H., & Xie, H. P. (2011). Study on the transmission and reflection of stress waves across joints. *International Journal of Rock Mechanics and Mining Sciences, 3*, 364–371.

Liang, W., Liu, H., Li, M. M., & Yue, G. W. (2020). Study on uniaxial/triaxial impact dynamic properties of structurally heterogeneous coal. *The Chinese Journal of Process Engineering, 21*(7), 10. (in Chinese).

Liu, K., Zhang, Q. B., Wu, G., Li, J. C., & Zhao, J. (2019b). Dynamic mechanical and fracture behaviour of sandstone under multiaxial loads using a Triaxial Hopkinson bar. *Rock Mechanics and Rock Engineering, 52*, 2175–2195.

Liu, K., & Zhao, J. (2021). Progressive damage behaviours of triaxially confned rocks under multiple dynamic loads. *Rock Mechanics and Rock Engineering, 54*, 3327–3358.

Liu, K., Zhao, J., Wu, G., Maksimenko, A., Haque, A., & Zhang, Q. B. (2020b). Dynamic strength and failure modes of sandstone under biaxial compression. *International Journal of Rock Mechanics and Mining Sciences, 128*, 104260.

Liu, P. F., Liu, K., & Zhang, Q. B. (2020c). Experimental characterisation of mechanical behaviour of concrete-like materials under multiaxial confinement and high strain rate. *Construction and Building Materials, 258*, 119638.

Liu, X. L., Liu, Z., Li, X. B., Gong, F. Q., & Du, K. (2020a). Experimental study on the effect of strain rate on rock acoustic emission characteristics. *International Journal of Rock Mechanics and Mining Sciences, 133*, 104420.

Liu, X. H., Xue, Y., Zheng, Y., & Gui, X. (2021). Research on energy release in coal rock fragmentation process under impact load. *Chinese Journal of Rock Mechanics and Engineering, 40*(S02), 11. (in Chinese).

Liu, Y. B., Yin, G. Z., Li, M. H., Zhang, D. M., & Zhao, H. G. (2019a). Mechanical properties and failure behavior of dry and watersaturated anisotropic coal under truetriaxial loading conditions. *Rock Mechanics and Rock Engineering, 53*(11), 4799–4818.

Lu, J., Yin, G. Z., Zhang, D., Gao, H., & Li, M. (2020a). True triaxial strength and failure characteristics of cubic coal and sandstone under different loading paths. *International Journal of Rock Mechanics and Mining Sciences, 135*, 104439.

Lu, J., Zhang, D., Huang, G., Xing, L., & Yin, G. Z. (2020b). Effects of loading rate on the compound dynamic disaster in deep underground coal mine under true triaxial stress. *International Journal of Rock Mechanics and Mining Sciences, 134*(10), 104453.

Luo, Y., Gong, H. L., Huang, J. H., Gang, W., Li, X. P., & Wang, S. (2022). Dynamic cumulative damage characteristics of deep-buried granite from Shuangjiangkou hydropower station under true triaxial constraint. *International Journal of Impact Engineering, 165*, 104215.

Ma, S. S., Chen, W. Z., & Zhao, W. S. (2021). Effects of axial static stress and confining pressure on the dynamic compressive behaviours of granite. *European Journal of Environmental and Civil Engineering, 25*, 795–812.

McGarr, A., & Gay, N. (1978). State of stress in the earth's crust. *Annual Review of Earth and Planetary Sciences*, *6*, 405–436. https://doi.org/10.1146/annurev.ea.06.050178.002201.

Mogi, K. (1971). Fracture and flow of rocks under high triaxial compression. *Journal of Geophysical Research, 76*(5), 1255–1269.

Mudau, A., Govender, R. A., & Stacey, T. R. (2016). A step towards combating rockburst damage by using sacrificial support. *Journal of the Southern African Institute of Mining and Metallurgy, 116*, 1065–1074.

Sato, K., Kawakita. M., Kinoshita, S (1981). The dynamic fracture properties of rocks under confining pressure. *Memoirs of the faculty of Engineering Hokkaido University*.

Seager, J. S. (1964). Pre-mining lateral pressures. *International Journal of Rock Mechanics and Mining Science & Geomechanics Abstracts, 1*(3), 413–419.

Shen, R. X, Li, H. R., Wang, E. Y., Chen, T. Q., Li, T. X., Tian, H., Hou, Z. H. (2020). Infrared radiation characteristics and fracture precursor information extraction of loaded sandstone samples with varying moisture contents. *International Journal of Rock Mechanics and Mining Sciences*, 130.

Si, X., Huang, L., Gong, F., Liu, X. L., & Li, X. B. (2020). Experimental investigation on influence of loading rate on rockburst in deep circular tunnel under true-triaxial stress

condition. *Journal of Central South University, 27*(10), 2914–2929.

Xiao, Y., Shan, J., Zheng, Q., Chen, B. S., & Shen, Y. L. (2009). Experimental studies on concrete filled steel tubes under high strain rate loading. *Journal of Materials in Civil Engineering, 21*(10), 569–577.

Xie, H. P., Zhu, J. B., Zhou, T., & Zhao, J. (2021). Novel three-dimensional rock dynamic tests using the true triaxial electromagnetic hopkinson bar system. *Rock Mechanics and Rock Engineering, 4*, 2079–2086.

Xu, S., Shan, J., Zhang, L., Zhou, L., Gao, G., Hu, S., & Wang, P. (2020). Dynamic compression behaviors of concrete under true triaxial confinement: An experimental technique. *Mechanics of Materials, 140*, 103220. https://doi.org/10.1016/j.mechmat.2019.103220.

Yin, G. Z., Li, M. H., Xu, J., Wang, W. Z., Li, W. P., Li, X., Song, Z. L., & Deng, B. (2015). A new Multi-functional true triaxial fluid-solid coupling experiment system and its applications. *Chinese Journal of Rock Mechanics and Engineering, 34*(012), 2436–2445. (in Chinese).

Yin, Z. Q., Li, X. B., Jin, J. F., He, X. Q., & Du, K. (2012). Failure characteristics of high stress rock induced by impact disturbance under confining pressure unloading. *Transactions of Nonferrous Metals Society of China, 22*, 175–184.

You, W., Dai, F., & Liu, Y. (2022). Experimental and numerical investigation on the mechanical responses and cracking mechanism of 3D confined single-flawed rocks under dynamic loading. *ScienceDirect, 14*, 477–493.

You, W., Dai, F., Liu, Y., Du, H. B., & Jiang, R. C. (2021). Investigation of the influence of intermediate principal stress on the dynamic responses of rocks subjected to true triaxial stress state. *International Journal of Mining Science and Technology, 31*, 913–926.